# Global Marching Technique for Predicting Separated Flows over Arbitrary Airfoils

Ahmad A. M. Halim*
*Air Force Institute of Technology*
*Wright-Patterson Air Force Base, Ohio*

## Introduction

THE aerodynamic design of a flight vehicle accounts for the drag, and the estimation of the drag is greatly affected by viscous effects. For flows of practical interest, the Reynolds number is sufficiently large for the flowfield to be divided into viscous and inviscid zones, e.g., the problem of flow past a wing. Different approaches are available for solving such a problem. Inherently, the Navier-Stokes formulations lead to an extremely stiff nonlinear system. Using an explicit algorithm to solve such problems results in the requirement of very small time-steps in order to satisfy the stability bounds. Therefore, many iterations and large amounts of computer time are required to reach the steady state. To remove the time-step restriction, fully implicit methods have been investigated. The implicit methods, however, still require many iterations to reach the steady state and consequently, require large computational costs.

The present work is a generalization and improvement of an earlier work developed for studying separated flows using boundary-layer-type equations. The improvements include extensions to a general coordinate system and use of a more general zonal technique for solving the coupled equations. In order to be able to consider arbitrary geometries, second-order-accurate (in space) conservative differences are generated by considering the integral formulation of the governing equations in a general coordinate system. The general coordinate system is handled in as general a manner as possible in order to allow for the use of either analytically or numerically generated coordinate systems.

The present work used a marching procedure for solving the approximate Navier-Stokes (ANS) equations in the viscous region coupled in a fully implicit manner with the elliptic inviscid equation. To demonstrate the independence of the scheme, as to the way the grid was generated, different grid generation techniques were employed (parabolic and algebric grid generation algorithms). Both orthogonal and nonorthogonal grids were used to predict the flow solutions for the J012 and NACA-0012 airfoils. New results were obtained for the J025 airfoil and a comparison with the experiment is shown.

## Analysis

The basic equations that describe the motion of laminar incompressible flow are the Navier-Stokes equations. These equations can be written in stream function-vorticity ($\psi$-$\omega$) form in general coordinates,

$$-J\omega=\frac{\partial}{\partial\xi}\left(\frac{\alpha}{J}\frac{\partial\psi}{\partial\xi}-\frac{\beta}{J}\frac{\partial\psi}{\partial\eta}\right)+\frac{\partial}{\partial\eta}\left(\frac{\psi}{J}\frac{\partial\psi}{\partial n}-\frac{\beta}{J}\frac{\partial\psi}{\partial\xi}\right) \quad (1)$$

and

$$J\frac{\partial\omega}{\partial t}+\frac{\partial\psi}{\partial\eta}\frac{\partial\omega}{\partial\xi}-\frac{\partial\psi}{\partial\xi}\frac{\partial\omega}{\partial\eta}=\frac{1}{Re}\left[\frac{\partial}{\partial\xi}\left(\frac{\alpha}{J}\frac{\partial\omega}{\partial\xi}-\frac{\beta}{J}\frac{\partial\omega}{\partial\eta}\right)+\frac{\partial}{\partial\eta}\left(\frac{\gamma}{J}\frac{\partial\omega}{\partial\eta}-\frac{\beta}{J}\frac{\partial\omega}{\partial\xi}\right)\right] \quad (2)$$

where

$$\alpha=x_\eta^2+y_\eta^2 \quad (3)$$

$$\beta=x_\xi x_\eta+y_\xi y_\eta \quad (4)$$

$$\gamma=x_\xi^2+y_\xi^2 \quad (5)$$

$$J=x_\xi y_\eta-x_\eta y_\xi \quad (6)$$

and $Re$ is the Reynolds number. If the chosen coordinate system is orthogonal, then $\beta$ is zero.

Defining the unit vectors in the $(\xi,\eta)$ coordinate system as $(e_1,e_2)$, the velocity vector $V$ can be expressed as

$$V=ue_1+ve_2 \quad (7)$$

where $u$ and $v$ are the components of $V$ defined as

$$u=\frac{\partial\psi}{\partial\eta} \quad (8)$$

$$v=-\frac{\partial\psi}{\partial\xi} \quad (9)$$

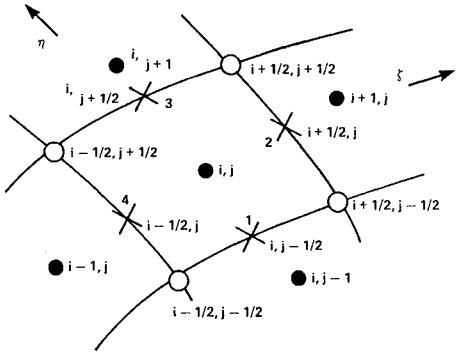


**Fig. 1 Differential element.**

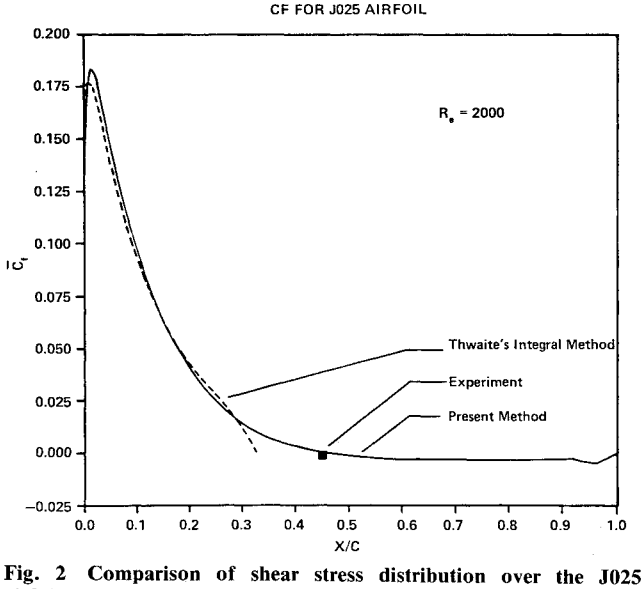


**Fig. 2 Comparison of shear stress distribution over the J025 airfoil.**

Received July 7, 1986; presented as Paper 87-0591 at the AIAA 25th Aerospace Sciences Meeting, Reno, NV, Jan. 12–15, 1987; revision received Feb. 15, 1987. This paper is declared a work of the U.S. Government and is not subject to copyright protection in the United States.

*Associate Professor, Department of Aeronautics and Astronautics. Senior Member AIAA.

The relation between the Cartesian velocity components $(u_c, v_c)$ and the present velocity components $(u, v)$ is

$$u_c = (x_\xi u + x_\eta v)/J \tag{10}$$

$$v_c = (y_\xi u + y_\eta v)/J \tag{11}$$

**Evaluation of the Pressure**

The momentum equations can be written as

$$\rho V \cdot \nabla V = -\nabla P - \mu \nabla^2 V \tag{12}$$

where $p$ is the pressure and $\rho$ is density. Multiplying the $x$-momentum equation by $dx$ and the $y$-momentum equation by $dy$ and adding the two to get a single equation for the pressure,

$$\rho \frac{\partial}{\partial x}\left(\frac{u_c^2+v_c^2}{2}\right)dx + \rho \frac{\partial}{\partial y}\left(\frac{u_c^2+v_c^2}{2}\right)dy - \rho v_c \frac{\partial v_c}{\partial x}dx$$
$$- \rho u_c \frac{\partial u_c}{\partial y} + \rho u_c \frac{\partial v_c}{\partial x}dy + \rho v_c \frac{\partial u_c}{\partial y}dx$$
$$= -\left(\frac{\partial P}{\partial x}dx + \frac{\partial P}{\partial y}dy\right) + \mu\left(\frac{\partial \omega}{\partial x}dy - \frac{\partial \omega}{\partial y}dx\right) \tag{13}$$

Eq. (13) can be written as

$$d\left[\rho\frac{V^2}{2} + P\right] + \rho\omega d\psi = \mu\left(\frac{\partial \omega}{\partial x}dy - \frac{\partial \omega}{\partial y}dx\right) \tag{14}$$

The Cartesian operators can be expressed in terms of the general coordinates as

$$\frac{\partial}{\partial x} = \frac{1}{J}\left(y_\eta \frac{\partial}{\partial \xi} - y_\xi \frac{\partial}{\partial \eta}\right) \tag{15}$$

$$\frac{\partial}{\partial y} = \frac{1}{J}\left(x_\xi \frac{\partial}{\partial \eta} - x_\eta \frac{\partial}{\partial \xi}\right) \tag{16}$$

Equation (13) is expressed in terms of the general coordinates as

$$d\left[\rho\frac{V^2}{2} + P\right] = -\rho\omega d\psi + \mu\left[\frac{\beta}{J}\frac{\partial \omega}{\partial \xi} - \frac{\gamma}{J}\frac{\partial \omega}{\partial \eta}\right]d\xi$$
$$+ \mu\left[-\frac{\beta}{J}\frac{\partial \omega}{\partial \eta} + \frac{\alpha}{J}\frac{\partial \omega}{\partial \xi}\right]d\eta \tag{17}$$

or in terms of $C_p$ (the pressure coefficient) as

$$d[V^2 + C_p] = -2\omega d\psi + \frac{2}{Re}\left[\left(\frac{\beta}{J}\omega_\xi - \frac{\gamma}{J}\omega_\eta\right)d\xi\right.$$
$$\left. + \left(-\frac{\beta}{J}\frac{\partial \omega}{\partial \eta} + \frac{\alpha}{J}\frac{\partial \omega}{\partial \xi}\right)d\eta\right] \tag{18}$$

**Inviscid Analysis**

The inviscid solution in the present work is obtained from an incompressible stream function representation of the inviscid flow region with zero vorticity. The boundary conditions for the inviscid region are, at the inflow boundary, $\xi = \xi_1$, $u = u_\infty$. On the interface, $\psi$ is known from the coupling between the viscous and inviscid zones, and for $\eta \to \infty$, $u \to u_\infty$. At the outer flow boundary, $\xi = \xi_0$, $\psi_x = 0$ (see Ref. 2 for more details).

A second-order-accurate conservative-difference scheme is generated for the stream function equation by integrating the equation around a differential element in the physical domain. The resulting algebraic system of equations is solved iteratively with the SLOR (successive line over relaxation) scheme. At each $\xi$ line in the computational domain, the finite-difference equation at each nodal point is

$$a_J \delta\psi_{J-1} + b_J \delta\psi_J + c_J \delta\psi_{J+1} = d_J \tag{19}$$

where the index $J$ denotes the grid position in the $\eta$ direction and $\delta\psi$ the change of $\psi$ between iterations, that is

$$\delta\psi = \psi^{n+1} - \psi^n \tag{20}$$

Along each $\xi$ line, a tridiagonal system of equations is solved using the Thomas algorithm.

**Viscous Analysis**

The flow in the viscous region is assumed to be governed by the ANS equations

$$\frac{\partial}{\partial \xi}(\omega\psi_\eta) - \frac{\partial}{\partial \eta}(\omega\psi_\xi) = \frac{1}{R_e}\frac{\partial}{\partial \eta}\left(\frac{\gamma}{J}\frac{\partial \omega}{\partial \eta}\right) \tag{21}$$

$$J\omega + \frac{\partial}{\partial \xi}\left(\frac{\alpha}{J}\frac{\partial \psi}{\partial \xi} - \frac{\beta}{J}\frac{\partial \psi}{\partial \eta}\right) + \frac{\partial}{\partial \eta}\left(\frac{\gamma}{J}\frac{\partial \psi}{\partial \eta} - \frac{\beta}{J}\frac{\partial \psi}{\partial \xi}\right) = 0 \tag{22}$$

These equations are to be solved in the viscous region.

The boundary conditions for the viscous equations are, at the surface

$$\eta = 0, \quad \psi = \psi_\eta = 0 \tag{23a}$$

at the interface

$$\eta = \eta_{IN}, \quad \psi = \psi_{IN} \text{(obtained from the coupling)}, \quad \omega = 0 \tag{23b}$$

at the inflow boundary

$$\xi = \xi_1, \quad \psi = \psi(\eta), \quad \omega = \omega(\eta) \tag{23c}$$

and at the outflow boundary, $\xi = \xi_0$ viscid/inviscid interaction is neglible.

Central finite-difference approximations are used everywhere except for the term $(\psi_\eta \delta\omega_\xi)$, which is treated as an upwind difference. That means that in the limit of the steady state, a second-order-accurate solution is obtained. At each $\xi$ line, the correction equations based on a Newton linearization procedure have the general form of

$$A\delta\psi_{I,J-1} + B\delta\psi_{I,J} + C\delta\psi_{I,J+1} + D\delta\omega_{I,J-1}$$
$$+ E\delta\omega_{I,J} + F\delta\omega_{I,J+1} = R_1 \tag{24a}$$

$$a\delta\psi_{I,J-1} + b\delta\psi_{I,J} + c\delta\psi_{I,J+1} + d\delta\omega_{I,J-1}$$
$$+ e\delta\omega_{I,J} + f\delta\omega_{I,J+1} = R_2 \tag{24b}$$

A block $(2\times2)$ tridiagonal Thomas algorithm is used, where in the forward pass the coefficients are calculated starting with the interface boundary conditions. The boundary condition at the surface and the coupling between the viscous and inviscid zones are treated in the same way as described in Ref. 2.

## Numerical Generation of Metric Coefficients

As explained, one way of generating a second-order-accurate conservative-differencing scheme includes calculating the metric coefficients and the Jacobian of the coordinate transformation at the center (in the transformed plane) of each side of the differential element shown in Fig. 1. On sides 1 and 3, the coefficients $\gamma/J$ and $\beta/J$ will be calculated, while $\alpha/J$ and $\beta/J$ will be calculated on sides 2 and 4. Using side 1 as an example, $\gamma_1$, $\beta_1$, and $J_1$ were

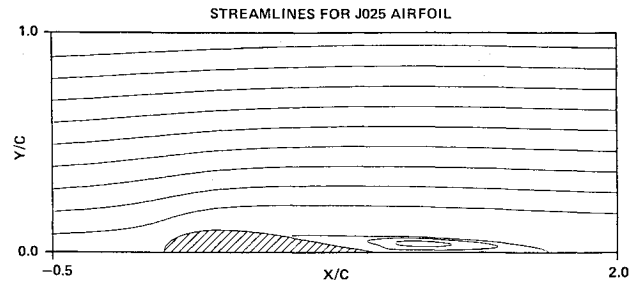


**Fig. 3 Streamline contours for flow past the J025 airfoil.**

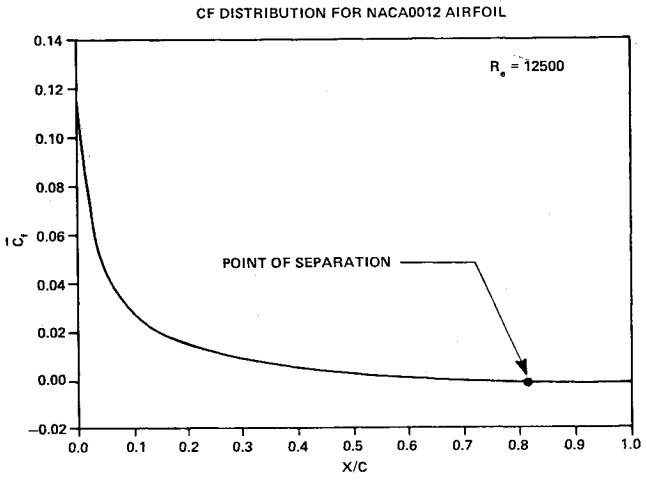


**Fig. 4 Skin-friction distribution for the NACA-0012 airfoil.**

previously defined as

$$\gamma_1 = x_{1\xi}^2 + y_{1\xi}^2 \tag{25}$$

$$\beta_1 = x_{1\xi}x_{1\eta} + y_{1\xi}y_{1\eta} \tag{26}$$

$$J_1 = x_{1\xi}y_{1\eta} - x_{1\eta}y_{1\xi} \tag{27}$$

Along side 1, $\Delta\eta = 0$; therefore,

$$\Delta x_1 = x_{1\xi}\Delta\xi_1 \tag{28}$$

or

$$x_{1\xi} = \frac{\Delta x_1}{\Delta\xi_1} \tag{29}$$

Using the subscripts in Fig. 1,

$$x_{1\xi_{i,j-1/2}} = \frac{x_{i+1/2,j-1/2} - x_{i-1/2,j-1/2}}{\Delta\xi} \tag{30}$$

where $\Delta\xi_1 = \Delta\xi_3 = \Delta\xi = \text{constant}$. Similarly,

$$y_{1\xi_{i,j-1/2}} = \frac{y_{i+1/2,j-1/2} - y_{i-1/2,j-1/2}}{\Delta\xi}$$

These central differences are second-order-accurate in space. Therefore, $\gamma_1$ can be represented to second-order accuracy as

$$\gamma_1 = \gamma_{i,j-1/2} = (x_{1\xi_{i,j-1/2}})^2 + (y_{1\xi_{i,j-1/2}})^2 \tag{31}$$

The coefficients $\beta$ and $J$ include the terms $x_{1\eta}$ and $y_{1\eta}$. $x_{1\eta}$ and $y_{1\eta}$ are calculated in the same manner as $x_{1\xi}$ and $y_{1\xi}$, and their second-order-accurate finite-difference representations are

$$x_{1\eta_{i,j-1/2}} = \frac{x_{i,j} - x_{i,j-1}}{\Delta\eta} \tag{32}$$

$$y_{1\eta_{i,j-1/2}} = \frac{y_{i,j} - y_{i,j-1}}{\Delta\eta} \tag{33}$$

Therefore, the second-order-accurate representations of $\beta_1$ and $J_1$ are

$$\beta_1 = \beta_{i,j-1/2} = (x_{1\xi_{i,j-1/2}})(x_{1\eta_{i,j-1/2}}) + (y_{1\xi_{i,j-1/2}})(y_{1\eta_{i,j-1/2}}) \tag{34}$$

$$J_1 = J_{i,j-1/2} = (x_{1\xi_{i,j-1/2}})(y_{1\eta_{i,j-1/2}}) - (x_{1\eta_{i,j-1/2}})(y_{1\xi_{i,j-1/2}}) \tag{35}$$

The finite-difference expressions for the metric coefficients and the Jacobian of the transformation at the center of the remaining element sides are derived analogously. Therefore, to generate the metric coefficients and Jacobians through the solution plane with central differences, the Cartesian coordinates of the algorithm solution points, the corners of the differential elements, and the points outside the boundaries must be known.

## Results and Discussion

The numerical algorithm discussed has been used to predict the flow over arbitrary airfoils. The first case was flow past the symmetrical Joukowski airfoil at zero angle of attack. For the case of the J012 airfoil, the choice of the grid is very critical for viscous computations over airfoils. There has been general agreement that C-type grids are the best for handling the trailing edge and wakes for airfoils. One clear advantage of the present formulation is the complete independence of the way in which the grid is generated. That means that the present scheme is capable of solving any type of grid. A C-type grid for J012 airfoil (see Fig. 1, Ref. 1) was implemented for the present work. Only half of the grid was used for the general computations due to the symmetry of the problem.

Figure 2 in Ref. 1 shows the friction coefficient ($\bar{C}_f$) over the surface of the airfoil at $Re = 2000$. The value of $\bar{C}_f$ in the vicinity of the leading edge of the airfoil is in complete agreement with the stagnation point flow solution ($\phi\eta\eta_w = 1.2326$). The hollow circles represent the present results while the solid circles represent those obtained using the Thwaites integral method. As seen from the graph, the two predictions are in complete agreement until before the point of flow separation. The Thwaites method predicts separation before the present method because the integral method of Thwaites completely neglects the interaction between the viscous and inviscid regions while the present method allows for it. As a side point, although the Thwaites method is an old method (1960), it still remains a very simple tool for predicting the boundary-layer parameters for flows with very weak interactions (attached flows). The values of $\bar{C}_f$ near the trailing edge of the airfoil were magnified on a larger scale to be able to see the solution in that region (Fig. 3, Ref. 1). The flow separated at 64% of the chord in accordance with the experimental data of Bussmann and Ulrich. The streamline contours are given in Fig. 4, Ref. 1. To test the algorithm for another severe case, an nonorthogonal grid (Fig. 5, Ref. 1) generated for the J025 airfoil was used to solve for the flow past the J025 airfoil. As a side notice, the grid is an adaptive grid based on the solution of the integral boundary-layer equation. Thwaites method was used first to generate the boundary-layer growth over the surface of the airfoil. That distribution of the boundary-layer thickness was used as an input for the grid generation code. The numerical results for that case are shown in Fig. 2. On that figure the values of $\bar{C}_f$ predicted using the Thwaites integral method

are shown as a dotted line and those predicted using the present method are shown as a solid line. The experimental prediction is shown as a solid square. Again, the present results and those predicted by the Thwaites method are in good agreement till before the point of separation for the same reasons explained before. As seen from the graph, the location of the point of separation is in agreement with the experimental prediction of Bussman and Ulrich. The streamlines for the J025 airfoil are shown in Fig. 3. This case is considered a massive separation case, since the dimension of the bubble is of the same order as the dimension of the body, which is an indication of the generality of the algorithm of handling massive separation problems without any difficulty. The last set of results are shown for NACA-0012 airfoil at $Re = 12{,}500$. An arbitrary C-type grid used for that case is shown in Fig. 8, Ref. 1. The values of $(\bar{C}_f)$ are shown in Fig. 4. From that figure, it is clear that the flow separation at $(X/C) = 0.8178$. Swanson and Turkel used a multistage time-stepping scheme for the Navier-Stokes equations to solve for that airfoil using a C-type grid. Their predictions indicated flow separation at $X/C \simeq 0.817$. On the other hand, Rubin reported flow separation at $X/C \simeq 0.84$ for $Re = 12{,}500$. It should be mentioned that the grid used by Rubin was an H-type grid, which is not highly recommended for viscous flow computation. The streamline contours are given in Fig. 10, Ref. 1. For higher Reynolds number values, the nature of the flow is not steady laminar. To be able to handle solutions for higher Reynolds numbers, the transition from laminar to turbulent must be accounted for in the numerical solution. That work is the subject of a current study.

## Concluding Remarks

The following statements provide a summary of the more important conclusions that can be extracted from the preceding text:

1) The governing equations are written in a general coordinate system, so flows past arbitrary airfoils can be solved using the present formulation.

2) Second-order-accurate (in space) conservative differences are generated by considering the integral formulation of the governing equations.

3) The algorithm used a marching procedure for solving the ANS equations in the viscous region, similar to the type of numerical solution used for the boundary-layer equations; thus, it can be classified as a boundary-layer-type scheme. Furthermore, the ANS equations have been efficiently coupling in a fully implicit manner with the inviscid stream function equation.

4) Solutions were obtained for J012, NACA-0012, and J025 airfoils.

5) For the J025 airfoil, the flow separated in agreement with the experimental data of Bussmann and Ulrich.

## References

[1]Halim, A.A.M., "A Global Marching Technique for the Prediction of Separated Flows over Arbitrary Airfoils," AIAA Paper 87-0591, 1987.

[2]Halim, A.A.M., "Development of an Iterative Boundary Layer-Type Solver for Axisymmetric Separated Flows," *AIAA Journal*, Vol. 24, Aug. 1986, pp. 1298–1304.

# Similarity of Ejector Wall-Pressure Distributions

M.S. Chandrasekhara* and A. Krothapalli†
*Florida State University, Tallahassee, Florida*
and
D. Baganoff‡
*Stanford University, Stanford, California*

## Introduction

THE mechanics of thrust augmentation, using ejectors, can be explained with the help of the pressure distribution found on the ejector surface. Often, the pressure distribution along the wall is also used to describe the mixing process that occurs inside the ejector duct. For example, the location at which the primary jet meets the ejector shroud can be easily obtained from the wall-pressure distribution. These distributions are generally plotted in terms of a normalized pressure coefficient defined as

$$C_p = \frac{p(x) - p_{amb}}{p_t - p_{amb}}$$

where $p(x)$ and $p_t$ denote the local surface pressure and throat pressure respectively while $p_{amb}$ represents the pressure in the ambient medium (see Fig. 1).

When the primary jet operates near or above the critical pressure ratio (stagnation pressure/ambient pressure), the pressure profiles exhibit different behavior for different operating pressure ratios. This observation was made by Quinn[1] for an axisymmetric ejector and by Hsia[2] for a rectangular jet ejector. The lack of similarity in the profiles was attributed to the different mixing phenomena that occur inside the duct for different pressure ratios, and this has been related[1,2] to the generation of "screech tones," which are commonly observed in free underexpanded jets, and their subsequent interaction with the primary jet.

Interestingly, the pressure distributions plotted in the same coordinates for multiple-jet ejectors show self-similarity for all operating conditions, including underexpanded nozzle-pressure ratios. This is because of the *absence* of strong acoustic interactions, which were observed by Hsia[2] for the case of a single-jet ejector. This Note was prompted by the conspicuous absence of these acoustic interactions in both subsonic and supersonic multiple jets.

## Description of the Facility and Experiment

The experiments carried out used the same blowdown facility and model as those described in Ref. 3. The jet assembly consisted of a linear array of rectangular jets of $0.3 \times 5.0$-cm exit dimensions mounted on a wedge with a 70-deg included angle (see Fig. 1). The jets were spaced at 2.4 cm apart. The shroud enclosing these jets was rectangular in cross section, and its area could be varied to simulate an ejector with an arbitrary area ratio $\mathcal{A}R$. Typically, $\mathcal{A}R = 20{:}1$, 26:1, and 33:1 were used. Also, the location of the

Received Aug. 19, 1985; revision received March 5, 1987. 

*Visiting Assistant Professor, Mechanical Engineering Department, FAMU/FSU College of Engineering. Senior Member AIAA.

†Professor, Mechanical Engineering Department, FAMU/FSU College of Engineering. Senior Member AIAA.

‡Professor, Department of Aeronautics and Astronautics. Member AIAA.